Graduate School of Oceanography Faculty Publications

Graduate School of Oceanography

1994

Coccolithophorid blooms in the global ocean

Christopher W. Brown
University of Rhode Island

James A. Yoder
University of Rhode Island, jimyoder@uri.edu

Follow this and additional works at: https://digitalcommons.uri.edu/gsofacpubs

Terms of Use

Coccolithophorid blooms in the global ocean

Christopher W. Brown[1] and James A. Yoder

Graduate School of Oceanography, University of Rhode Island, Narragansett

Abstract. The global distribution pattern of coccolithophorid blooms was mapped in order to ascertain the prevalence of these blooms in the world's oceans and to estimate their worldwide production of $CaCO_3$ and dimethyl sulfide (DMS). Mapping was accomplished by classifying pixels of 5-day global composites of coastal zone color scanner imagery into bloom and nonbloom classes using a supervised, multispectral classification scheme. Surface waters with the spectral signature of coccolithophorid blooms annually covered an average of 1.4×10^6 km^2 in the world oceans from 1979 to 1985, with the subpolar latitudes accounting for 71% of this surface area. Classified blooms were most extensive in the Subarctic North Atlantic. Large expanses of the bloom signal were also detected in the North Pacific, on the Argentine shelf and slope, and in numerous lower latitude marginal seas and shelf regions. The greatest spatial extent of classified blooms in subpolar oceanic regions occurred in the months from summer to early autumn, while those in lower latitude marginal seas occurred in midwinter to early spring. Though the classification scheme was efficient in separating bloom and nonbloom classes during test simulations, and biogeographical literature generally confirms the resulting distribution pattern of blooms in the subpolar regions, the cause of the bloom signal is equivocal in some geographic areas, particularly on shelf regions at lower latitudes. Standing stock estimates suggest that the presumed *Emiliania huxleyi* blooms act as a significant source of calcite carbon and DMS sulfur on a regional scale. On a global scale, however, the satellite-detected coccolithophorid blooms are estimated to play only a minor role in the annual production of these two compounds and their flux from the surface mixed layer.

Introduction

Coccolithophorids are an abundant and widely distributed component of the marine phytoplankton [*Gaarder*, 1971; *McIntyre and Be*, 1967; *Okada and McIntyre*, 1977] and are thought to play an important role in the oceanic carbon and sulfur cycles through their production of $CaCO_3$ coccoliths and dimethyl sulfide (DMS), the dominant precursor for cloud condensation nuclei in the maritime atmosphere. As one of the principal producers of DMS among the phytoplankton [*Andreae*, 1986; *Keller*, 1989], coccolithophorids may act as a significant biogenic source of sulfur for the atmosphere and may influence regional albedo via increased cloud formation [*Bates et al.*, 1987a; *Charlson et al.*, 1987]. Their coccolith production affects the air-to-sea carbon dioxide flux by increasing the pCO_2 in the surface layer [*Sarmiento et al.*, 1988; *Taylor et al.*, 1991] and constitutes a major source of calcareous sediments [*Bramlette*, 1958], which serve as a long-term carbon sink.

The biogeochemical influence of coccolithophorids is probably most pronounced when they occur in "bloom" proportion, where cell concentrations of up to 115 million cells per liter have been measured [*Berge*, 1962]. Yet little is known of how prevalent these blooms are in the global ocean. To estimate the magnitude of bloom-produced

CaCO_3 and DMS in the ocean relative to other sources and to assess their effect on regional CO_2 dynamics and planetary albedo, the large-scale spatial and temporal characteristics of these blooms must be known.

Coccolithophorid blooms have been observed and sampled in temperate and Subarctic latitudes of the North Atlantic [*Balch et al.*, 1991; *Holligan and Groom*, 1986; *Holligan et al.*, 1983], but little is known of their distribution pattern elsewhere in the world oceans. Satellite imagery provides the synoptic and repeated coverage appropriate to address this global-scale question. Their blooms can be distinguished from most other water conditions in visible satellite imagery owing to their high ocean volume reflectance in the surface layer, caused principally by the presence of their detached coccoliths [*Ackleson and Holligan*, 1989; *Balch et al.*, 1991]. We used the relatively unique spectral signature of coccolithophorid blooms to detect their presence in global composites of coastal zone color scanner (CZCS) imagery in order to determine their distribution pattern in time and space and to estimate the magnitude and periodicity of their $CaCO_3$ and DMS production.

Methods and Materials

The distribution pattern of major coccolithophorid blooms in the surface waters of the world oceans was mapped by classifying picture elements (pixels) of 5-day global composites of Nimbus 7 CZCS imagery dating from 1978 to 1986 into coccolithophorid bloom and nonbloom classes based on their mean normalized water-leaving radiances [*Gordon et al.*, 1988a] using a supervised, multispectral classification

---

```
┌─────────────────────────────────────┐
│   Coastal Zone Color Scanner        │
│   5-Day Global Composites           │
│                                     │
│   Normalized Water-Leaving Radiances│
│   November 1978 - June 1986         │
│   20 km Resolution                  │
└─────────────────────────────────────┘
                  ↓
┌─────────────────────────────────────┐
│   Sub - Sample Images               │
│   (2 x 2)                           │
└─────────────────────────────────────┘
                  ↓
┌─────────────────────────────────────┐
│   Classify Image                    │
│                                     │
│   Supervised Training               │
│   Multispectral Parallelepiped Scheme│
└─────────────────────────────────────┘
                  ↓
┌─────────────────────────────────────┐
│   Morphological Filter              │
└─────────────────────────────────────┘
         ↓                    ↓
Monthly Composite Images    Frequency of Blooms
                            ─────────────────────
                            Total Number of Observations
                                      ↓
                            Relative Frequency of
                            Coccolithophorid Bloom Occurrence
```
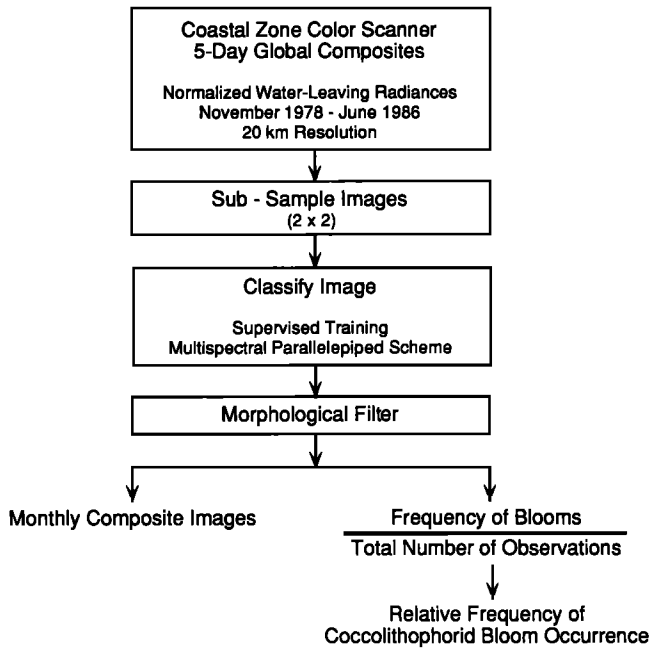
Figure 1. Flow chart of the methodology for processing and classifying global composites of visible CZCS imagery into coccolithophorid bloom and non-coccolithophorid bloom classes.

scheme. A classified bloom in this study was defined as a detectable entity that possessed spectral characteristics similar to coccolithophorid blooms that had been confirmed by in situ sampling. Any mention of a bloom in this paper refers to a coccolithophorid bloom unless otherwise specified.

Image Processing

Figure 1 outlines the methodology followed to process and classify the imagery. Images of 5-day mean normalized water-leaving radiances (nLw 440, nLw 520, and nLw 550) and aerosol radiance (La 670) from level 3 postage stamp (PST) files of the NASA CZCS global data set were rectified to a cylindrical equidistant projection and subsampled by 2 × 2 decimation to provide a spatial resolution of ≈40 km. The PST files are composed of averaged geophysical parameters from valid level 2b pixels (≈4-km resolution), with supporting image count and pixel sample size, binned to a fixed, linear latitude-longitude array [*Feldman et al.*, 1989]. The imagery had been atmospherically corrected with a multiple atmospheric scattering algorithm using the default maritime aerosol epsilon values [*Gordon et al.*, 1988a]. Clouds and sun glint had been masked, and scenes with excessively high aerosol radiance or low sun angles were excluded during initial processing at NASA.

Classification of Imagery

The mean radiance images served as input for a supervised, parallelepiped classification algorithm. A parallelepiped algorithm classifies an object by comparing the object's feature(s), in this case spectral, to class (decision) boundaries that form a parallelogram in two-dimensional feature space [*Schowengerdt*, 1983]. The classification algorithm was developed by first empirically determining the spectral signatures of coccolithophorid blooms and various common,

nonbloom conditions and then establishing decision boundary values that would allow the blooms to be spectrally distinguished from these other conditions.

Spectral signatures of coccolithophorid blooms, "clear" blue water, sediment-laden water, "whitings" (suspended lime muds [*Shinn et al.*, 1989]), and unmasked clouds (including cloud "ringing") were ascertained by extracting the normalized water-leaving and aerosol radiances from pixels located at "training sites" centered on portions of level 2b CZCS imagery identified to each condition (Table 1, Figure 2). The training site imagery had been processed similarly to the PST imagery. Most training sites were located in the North Atlantic, and those for nonbloom conditions were selected by contextual, though not necessarily verified, evidence. Training sites of sediment-laden water were located at or near river mouths. Those for whitings came from the Bahamas and the Persian Gulf, both areas renowned for this phenomenon [see *Robbins and Blackwelder*, 1992]. The eight coccolithophorid bloom training sites (n = 1276 pixels) were positioned in the *Emiliani huxleyi* (Lohmann) Hay et Mohler bloom sampled by *Holligan et al.* [1983] and in the high-reflectance patches in and adjacent to the Gulf of Maine where *E. huxleyi* blooms were sampled in subsequent years [*Ackleson and Holligan*, 1989; *Balch et al.*, 1991].

Five feature characters were chosen: nLw 440, nLw 550, nLw 440/nLw 520, nLw 440/nLw 550, and nLw 520/nLw 550. Their selection was based on the suite of characters that proved least redundant in separating the spectral signatures of the various conditions. The mean and standard deviation for each feature character of the bloom and the other spectrally defined conditions, with radiance values less than sensor saturation (2.55 mW cm^{-2} μm^{-1} sr^{-1}), are presented in Table 2.

Decision boundaries for each of the feature characters were set to values that would both exclude the greatest percentage of nonbloom conditions and include the maximum percentage of blooms. The boundary value(s) for each feature character was as follows: $1.10 < nLw$ 440 < 2.55, $0.80 \leq nLw$ 550 < 2.55, $0.95 \leq nLw$ 440/nLw 520 ≤ 1.50, $1.00 < nLw$ 440/nLw 550 < 2.00, $1.00 \leq nLw$ 520/nLw 550 ≤ 1.60, with radiances in units of mW cm^{-2} μm^{-1} sr^{-1}. An La 670 threshold (1.10 mW cm^{-2} μm^{-1} sr^{-1}), slightly greater than twice that of a clear atmosphere [*Gordon et al.*, 1988b], was set to exclude atmospheric "haze."

The decision boundaries were incorporated into a nonparametric parallelepiped algorithm which assigned nonland pixels to either coccolithophorid bloom or non-coccolithophorid bloom classes by comparing the radiance values of individual pixels to the decision boundaries set for each of the five spectral feature characters.

To evaluate the performance of the decision boundaries in separating the different classes, "test site" pixels (Table 1) were classified, and the percentages of correct and incorrect classifications were calculated on the basis of their previous assignment. Like training site pixels, test site pixels provided a representative spectral signature for each of the various conditions, but their radiances were not consulted when the decision boundaries were established. Test sites were located in the vicinity of, but did not overlap, their corresponding training sites, to avoid differences in aerosol characteristics. To determine the effect of reduced spatial

Table 1. Center Coordinates and Dates of Training and Test Sites Used to Establish Spectral Signatures for Coccolithophorid Bloom and Nonbloom Conditions

Date			Coordinates	
Julian Day	Year	Type	Training Site	Testing Site
153	1983	Clr	70.81°W, 39.54°N[a]	71.05°W, 38.48°N[a]
180	1983	Clr	66.43°W, 43.49°N[b]	58.72°W, 46.59°N[c]
181	1983	Clr	63.96°W, 42.75°N[c]	62.05°W, 42.48°N[c]
182	1983	Clr	60.13°W, 43.49°N[c]	62.05°W, 42.48°N[c]
191	1983	Clr	64.24°W, 41.03°N[c]	65.10°W, 40.52°N[a]
188	1979	Coc	64.28°W, 42.40°N[c]	63.69°W, 42.55°N[c]
147	1982	Coc	8.45°W, 48.25°N[d]	6.85°W, 48.13°N[d]
148	1982	Coc	8.45°W, 48.25°N[d]	6.85°W, 48.13°N[d]
149	1982	Coc	8.53°W, 48.29°N[d]	6.92°W, 48.13°N[d]
153	1983	Coc	68.93°W, 42.24°N[b]	68.39°W, 41.54°N[b]
160	1983	Coc	69.13°W, 42.59°N[b]	69.44°W, 43.14°N[b]
180	1983	Coc		69.29°W, 43.14°N[b]
		Coc		68.29°W, 42.75°N[b]
181	1983	Coc	69.01°W, 42.44°N[b]	67.84°W, 42.36°N[b]
		Coc		69.05°W, 41.89°N[b]
		Coc		67.33°W, 42.63°N[b]
182	1983	Coc	68.93°W, 42.01°N[b]	68.15°W, 42.16°N[b]
		Coc		68.35°W, 42.52°N[b]
194	1983	Haz	69.25°W, 42.16°N[b]	63.65°W, 43.61°N[c]
210	1983	Haz	69.25°W, 41.61°N[a]	70.19°W, 40.71°N[a]
247	1985	Red	73.63°W, 39.07°N[a]	73.75°W, 39.58°N[a]
125	1979	Sed	53.85°W, 6.24°N[e]	53.50°W, 5.81°N[e]
164	1979	Sed	48.69°W, 1.94°N[e]	53.03°W, 5.81°N[e]
177	1979	Sed	68.70°W, 48.54°N[f]	69.76°W, 47.76°N[f]
185	1979	Sed		69.76°W, 47.76°N[f]
202	1979	Sed	52.68°W, 5.58N[e]	53.58°W, 5.89°N[e]
		Sed		52.91°W, 5.66°N[e]
208	1979	Sed	53.30°W, 5.77°N[e]	56.24°W, 6.20°N[e]
		Sed	47.82°W, 0.22°S[e]	53.54°W, 5.97°N[e]
208	1979	Sed	56.16°W, 6.01°N[e]	52.09°W, 5.03°N[e]
273	1985	Sed	70.62°W, 41.11°N[a]	71.05°W, 41.22°N[e]
004	1979	Wht	50.82°E, 28.15°N[g]	49.27°E, 27.89°N[g]
015	1979	Wht	50.68°E, 27.78°N[g]	53.95°E, 24.51°N[g]
028	1979	Wht	50.05°E, 28.09°N[g]	50.78°E, 26.39°N[g]
032	1979	Wht	50.21°E, 28.95°N[g]	50.78°E, 26.39°N[g]
023	1980	Wht	71.67°W, 21.15°N[h]	
024	1980	Wht		71.67°W, 21.15°N[h]

Types are Cir, clear water; Coc, coccolithophore bloom; Haz, aerosal haze; Sed, suspended sediments; Red, "red" water condition; Wht, whitings. See text for further explanation.

[a]New York Bight or Slope Water off the northeastern United States; western North Atlantic.
[b]Gulf of Maine; western North Atlantic.
[c]Nova Scotia shelf or slope; western North Atlantic.
[d]Celtic Shelf; eastern North Atlantic.
[e]Coastal waters of northeastern South America; equatorial North Atlantic.
[f]St. Lawrence River; western North Atlantic.
[g]Persian Gulf.
[h]Bahamas, equatorial North Atlantic.

resolution between the training pixels (4 km) and the PST imagery (20 km) on classification performance, 500 mean radiance values for each condition were first calculated from 2^ν randomly chosen test site pixels, where ν ranged from 0 to 6, and then classified. For these simulations, we assumed that pixels binned into a PST image represented a random sampling of radiances from a given condition.

Postclassification Processing

A postclassification morphological erosion filter [*Jain*, 1989; *Simpson*, 1992], which deleted individual classified bloom pixels if surrounded by two or fewer bloom pixels in a 3 × 3 pixel area, was used to remove atmospheric artifacts. "Monthly" composites for each year were produced by
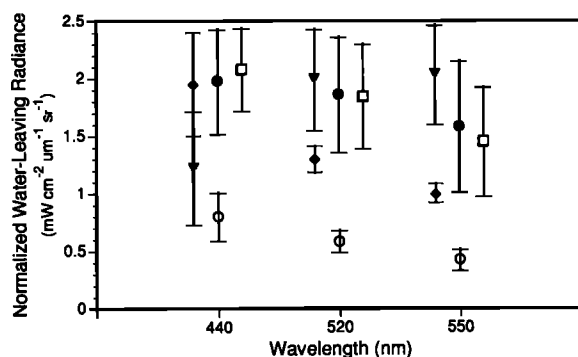
Figure 2. Mean ($\pm\sigma$) normalized water-leaving radiances (nLw) for coccolithophorid blooms (solid circles), "clear" blue water (open circles), haze (solid diamonds), sediments (solid triangles), and whitings (open squares) at CZCS band wavelengths.

combining six (or seven for December) sequential 5-day classified images in such a way as to indicate the location of all classified coccolithophorid blooms detected during that interval. Monthly maps of the relative frequency of bloom occurrence were also created from the 5-day classified imagery by dividing the total number of times blooms were present at a location (= pixel) by the total number of weekly observations recorded at that location. These monthly composites served as "building blocks" for annual and climatological composites.

The surface areas of classified blooms and the exposed sea surface of the world oceans were calculated from the monthly and annual composites by multiplying pixel area by the frequency of each pixel type in 10° latitudinal bands [*Brown*, 1993]. The area of exposed sea surface was not spatially registered. This measure of sea surface visibility, often referred to in this paper simply as visibility, is presented as the percentage of the total sea surface area in a geographic region.

The nonparametric Spearman rank correlation and Mann-Whitney U tests [*SAS Institute*, 1985] were used to examine the correlations between the usually nonnormally distributed variables or to detect statistical differences in their means.

Image Coverage

Imagery coverage varied temporally and spatially during the CZCS mission. In general, the frequency of coverage was highest in the first full 3 years (1979–1981) and then decreased [*McClain et al.*, 1990]. Spatial coverage was concentrated in coastal regions at midlatitudes of the northern hemisphere. The mean number of images and valid level 2 pixels $\pm$ standard deviation in each 5-day global composite classified in this study were 1.2 $\pm$ 0.15 days and 18 $\pm$ 3.31 pixels ($n = 538$).

Results

Classification Performance

The simulations to evaluate the efficacy of the classifier revealed that the number of both omissions (i.e., test bloom pixels excluded during classification from the bloom class) and commissions (i.e., nonbloom test pixels incorrectly classified into the bloom class) generally decreased as the spatial resolution of the imagery decreased (Figure 3). The combined percentages of commissions and omissions decreased to <3% when the simulated sample size (2ⁿ) was 16 or equivalent to a spatial resolution of 16 km². Noting that an average of 18 level 2 pixels (from a nominal maximum of 25) were binned to compute the mean radiance of a single 5-day PST pixel, these simulation results imply that most pixels are accurately classified.

Neglecting whitings for the moment, sediment and atmospheric haze were the only nonbloom conditions misclassified as blooms during testing simulations. This result is inevitable given the overlap of the spectral signatures of these conditions (Figure 2). Yet in the classified imagery, river plumes and their entrained sediments were often separable from blooms, as illustrated by their omission from all or most of the deltas of the Amazon, Orinoco, and Ganges rivers (Plate 1). In regard to atmospheric artifacts, sensor overshoot [*Mueller*, 1988], which affects a band 10 km or less downscan of land or clouds, poses minimal problems owing to the large scale of the imagery and the postclassification filtering. In addition, our results do not reveal any presence of the bloom signal along the Intertropical Convergence Zone, a region of potentially numerous unmasked clouds, implying that the bloom signals at zones of peak precipita-

Table 2. Training Site Spectral Statistics of the Environmental Conditions When CZCS Band 3 (550 nm) Was Not Saturated

Type	n	nLw 440	nLw 550	$\dfrac{nLw440}{nLw520}$	$\dfrac{nLw440}{nLw550}$	$\dfrac{nLw520}{nLw550}$
Clr	1435	0.80 ± 0.20	0.42 ± 0.87	1.4 ± 0.30	2.0 ± 0.58	1.4 ± 0.19
Coc	1095	1.92 ± 0.41	1.43 ± 0.42	1.1 ± 0.14	1.4 ± 0.27	1.3 ± 0.11
Haz	360	1.95 ± 0.44	0.99 ± 0.07	1.5 ± 0.29	2.0 ± 0.43	1.3 ± 0.07
Red	180	1.08 ± 0.15	1.24 ± 0.08	1.0 ± 0.11	0.9 ± 0.13	0.9 ± 0.06
Sed	1189	1.17 ± 0.48	1.92 ± 0.39	0.6 ± 0.20	0.6 ± 0.27	1.0 ± 0.15
Str	136	0.40 ± 0.26	0.82 ± 0.19	0.5 ± 0.16	0.5 ± 0.41	1.1 ± 0.61
Wht	838	2.06 ± 0.35	1.40 ± 0.43	1.2 ± 0.33	1.6 ± 0.67	1.3 ± 0.14

All values are means $\pm$ standard deviations. Types are Clr, clear water; Coc, coccolithophorid bloom; Haz, atmospheric "haze"; Red, "red" water condition; Sed, sediments; Str, river outflow; and Wht, whitings; nLw λ is normalized water-leaving radiance, in units of mW cm^{-1} μm^{-1} sr^{-1}.
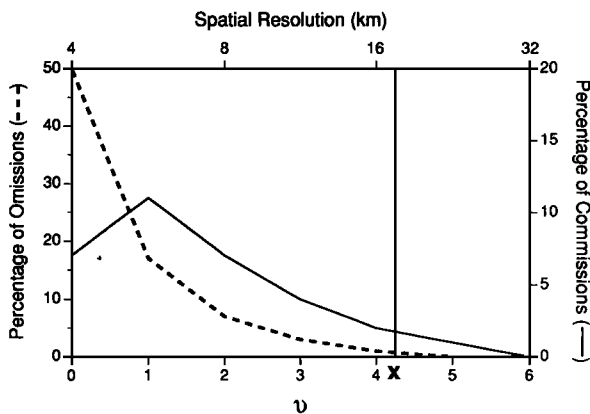
Figure 3. Classification performance at different spatial resolutions. The spectral signatures of bloom and nonbloom conditions at different pixel spatial resolutions were simulated by increasing the sample size ($n = 2^v$) of pixels used to compute the mean radiance value of a single PST pixel. The mean number of level 2b pixels comprising all valid PST pixels in this study, that is, 18, is denoted by the vertical line at X. Omissions indicate the percentage of test bloom pixels excluded from the bloom class after classification, and commissions indicate the percentage of nonbloom pixels incorrectly included in the classified bloom class. These results do not include the testing of whitings.

tion at subpolar latitudes, that is, 45°–50° [*Wallace and Hobbs*, 1977], are not due to unmasked clouds. Nor were classified blooms evident off northwestern Africa [*Durkee et al.*, 1991], indicating that mineral aerosols, at least those from the Sahara Desert, are excluded.

Whitings were spectrally indistinguishable from cocco-lithophorid blooms using the present classification scheme. The bloom signals appearing in the Bahamas and the Persian Gulf are by definition, as designated during training of the classification algorithm, due to the presence of whitings. As a consequence of the algorithm's inability to completely separate bloom from nonbloom conditions, a classified bloom does not necessarily represent the presence of a coccolithophorid bloom, and we distinguish between substantiated blooms and classified blooms in the following sections.

Postclassification filtering of classified bloom patches consisting of 3 or fewer pixels in a 3 × 3 pixel area further reduced the risk of incorrectly grouping atmospheric haze as a bloom yet also deleted an unknown quantity of actual blooms contiguously measuring less than 4800 km^2. Filtering often decreased the area of classified blooms in monthly composites by 50% or more.

Geographical Occurrence of the Coccolithophorid Bloom Signal

Surface waters with spectral signatures similar to that of *E. huxleyi* coccolithophorid blooms annually covered an average of 1.4×10^6 km^2 in the global ocean from 1979 to 1985, with subpolar latitudes accounting for 71% of this surface area (Table 3, Plate 1). Classified blooms were most extensive, both in absolute area and on a per area basis, in the Subarctic North Atlantic. Large expanses, with annual means of $\geq 100,000$ km^2, were also detected in the subpolar North Pacific and the southern ocean, primarily on the Argentine shelf and slope. Smaller classified blooms in the subpolar latitudes were observed off Chile and New Zealand. Classified blooms in the equatorial belt (10°N to 10°S) and the subtropical gyres (10°–40°N, 10°–40°S) were limited in spatial extent, with the exception of the South
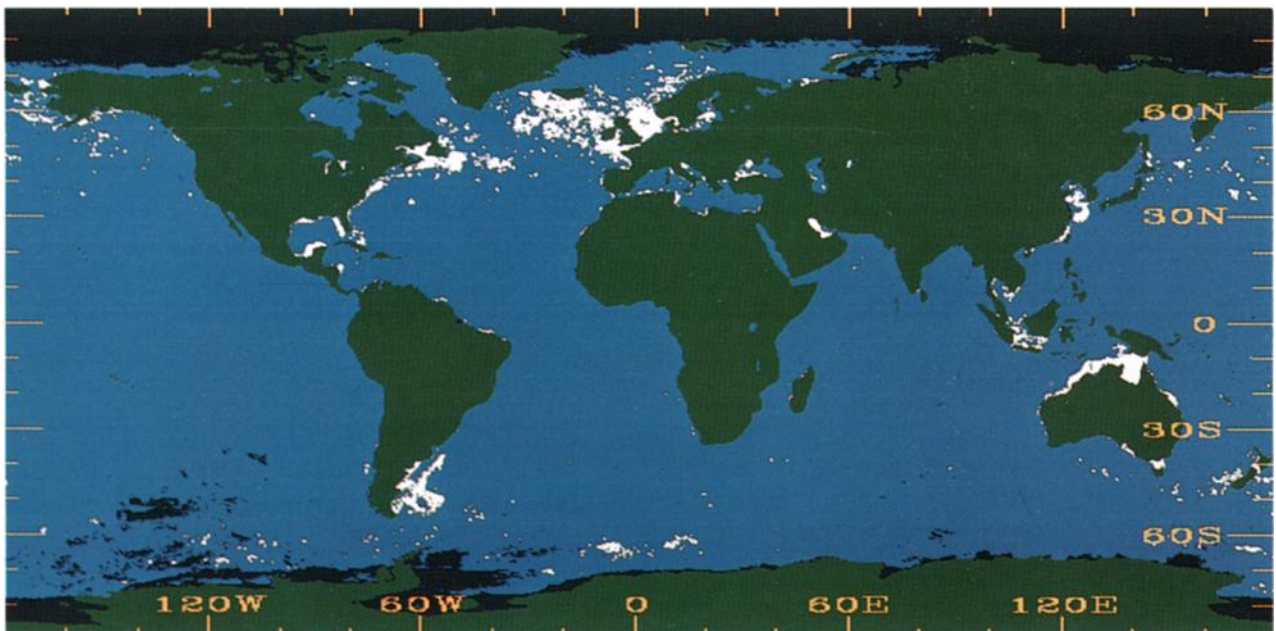

Plate 1. Climatology of classified coccolithophorid blooms (measuring >4800 km^2) for the world's oceans in CZCS imagery dating from November 1978 to June 1986. The maximum spatial extents of blooms detected during this period are displayed. The coccolithophorid bloom class is white, the noncoccolithophorid bloom class is blue, and the land is green. Black indicates areas lacking image coverage.

Table 3. Annual Mean Surface Area Covered by Classified Coccolithophorid Blooms in Regions of the Global Ocean

Region	Area, $\times 10^6$ km^2	Mean Bloom Surface Area $\pm$ s.d., $\times 10^3$ km^2
Equatorial Belt (10°N–10°S)		
Pacific	35.5	0.2 $\pm$ 0.57
Atlantic	13.0	16 $\pm$ 20.0
Indian	14.3	3 $\pm$ 2.6
Total and mean	62.8	20 $\pm$ 19.0
Subtropical Gyres (10°–40°N, 10°–40°S)		
North Pacific	40.7	18 $\pm$ 32.8
South Pacific	45.6	51 $\pm$ 27.1
North Atlantic	20.1	100 $\pm$ 41.6
South Atlantic	20.4	17 $\pm$ 19.5
North Indian	4.7	10 $\pm$ 2.8
South Indian	29.1	140 $\pm$ 47.4
Total and mean	160.6	330 $\pm$ 116.0
Subarctic (40°–60°N for Pacific, 40°–70°N for Atlantic)		
North Pacific	13.0	100 $\pm$ 138.0
North Atlantic	13.0	630 $\pm$ 818.0
Total and mean	26.0	730 $\pm$ 945.0
Subantarctic (40°–50°S)		
Circumpolar	31.1	170 $\pm$ 113.0
Antarctic (50°–70°S)		
Circumpolar	42.9	110 $\pm$ 82.6
Global Ocean		
Total and mean	323.4	1400 $\pm$ 1100

Indian, North Atlantic, and South Pacific gyres, where total annual bloom sizes averaged 140,000, 100,000, and 51,000 km^2, respectively (Table 3). Classified blooms in these lower latitudes were also generally restricted to waters over the continental shelves. For example, the majority of Indian Ocean classified blooms were located in the Timor Sea and on the northwest shelf of Australia (Plate 1). Blooms were negligible or absent from open ocean waters in the equatorial belt of all oceans.

Large expanses of the bloom signal were also detected in numerous lower latitude marginal seas, including the Yellow and East Chinese seas, the shelf regions of the Gulf of Mexico, the Arafura Sea and Gulf of Carpentaria, and the northwestern shelf of Australia (Plate 1). The mean annual total surface area of the bloom's signal in several marginal seas was large, equaling or exceeding the extent within numerous oceanic regions (Table 4). The Arafura Sea–Gulf of Carpentaria and the North Sea possessed the highest total bloom surface areas of all water bodies. Bloom signals, though less extensive, were also observed in the Great Lakes, Persian Gulf, Hudson Bay, and Norwegian, Baltic, Mediterranean, Black, Caspian, Chukchi, Bering, Java, and South China seas.

Contours of the relative frequency of classified bloom occurrence were superimposed on maps of sample size for climatological March, June, September, and December (Plate 2a–2d) to indicate the probability of monthly bloom "appearance" in the different regions of the world over the seasonal cycle and to convey the level of confidence associated with these probabilities. The white and light blue

contours indicate the areas where classified blooms occurred at a relative frequency of ≥ 0 and $\geq 50\%$, respectively. The total number of weekly observations at a location, that is, the denominator in the calculation of relative frequency of bloom occurrence, was color coded. The number of observations in oceanic regions at high latitudes never exceeded 15, with sample sizes of less than 5 common.

In December (Plate 2a), classified blooms occurred with high relative frequencies in the southern hemisphere off the Chilean coast and in the Patagonian region off Argentina, with patches of lower relative occurrence located off New Zealand and southern Australia. Smaller patches in the southern ocean at approximately 60°S along the coast of northern Australia and in the Indonesian seas achieved high relative frequencies, although they were derived from only one to five images. In the northern hemisphere, classified blooms consistently appeared throughout the $7\frac{1}{2}$ years in the well-sampled regions of the Persian Gulf, Mediterranean Sea, Atlantic coast of Honduras, northern Caribbean, and shelf regions within the Gulf of Mexico. The majority of classified blooms were detected in the poorly represented area between the southern Yellow Sea and the northern South China Sea only during 1979 and 1980. The pattern for December distribution of classified blooms remained essentially the same in January, with the exception of the appearance of blooms in the Celtic Sea and in the southern ocean at 12°E, 62°S (in 1980). By February the probability of bloom occurrence off Argentina had decreased considerably, though blooms to the west of South Georgia Island remained. Various patches of low-frequency occurrence were evident in the Mediterranean Sea and the Gulf of Alaska.

In March (Plate 2b), all signals along $\approx 60°S$ except for a relatively large patch at 7°W, 64°S (that occurred only in 1980) had disappeared. No classified blooms were evident along the outer Argentine shelf, though some still persisted closer inshore. Bloom signals first appeared on the northwest shelf of Australia, in the Arafura Sea and Gulf of Carpentaria, and in the Coral Sea during March and persisted there for several months. Areas of low relative bloom frequency were still present in the southern Yellow Sea and the Persian Gulf in the northern hemisphere but had diminished in spatial extent compared to those in preceding months. Small patches with low relative frequencies of occurrence (15%) were also detected in the well-represented central Arabian Sea and the western Indian Ocean and were still evident in the subtropical-tropical western North Atlan-

Table 4. Annual Mean Surface Area Covered by Classified Coccolithophorid Blooms of Selected Marginal Seas

Region	Area, $\times 10^6$ km^2	Mean Bloom Surface Area $\pm$ s.d. $\times 10^3$ km^2
Gulf of Mexico	1.7	230 $\pm$ 112.0
North Sea	1.0	240 $\pm$ 249.0
Arafura Sea and Gulf of Carpentaria	2.7	1100 $\pm$ 893.0
Yellow Sea	0.8	73 $\pm$ 107.0
Indonesian seas*	6.6	110 $\pm$ 116.0

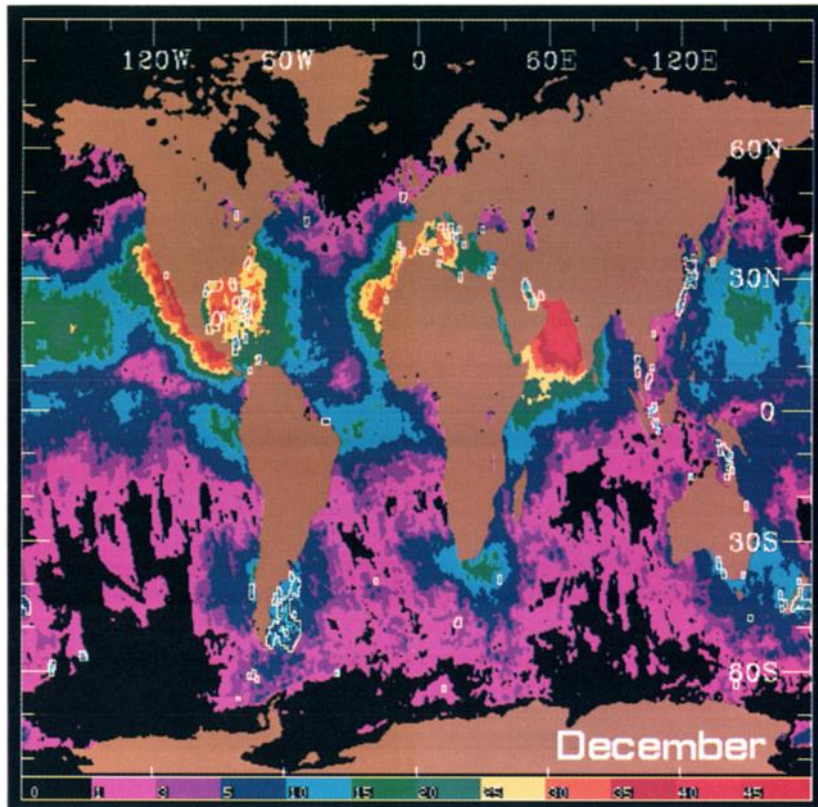*Includes the Gulf of Thailand and the South China and Java seas.

Plate 2a. Relative frequency of classified coccolithophorid bloom occurrence superimposed on a map of sample size, that is, number of 5-day composites, for climatological December. White and light blue contours indicate relative frequencies of bloom occurrence of ≥ 0 and $\geq 50\%$, respectively. Sample size is color coded according to the color bar given. Maximum sample size (n_{max}) = years $\times$ 5-day composites per month. December n_{max} = 56.
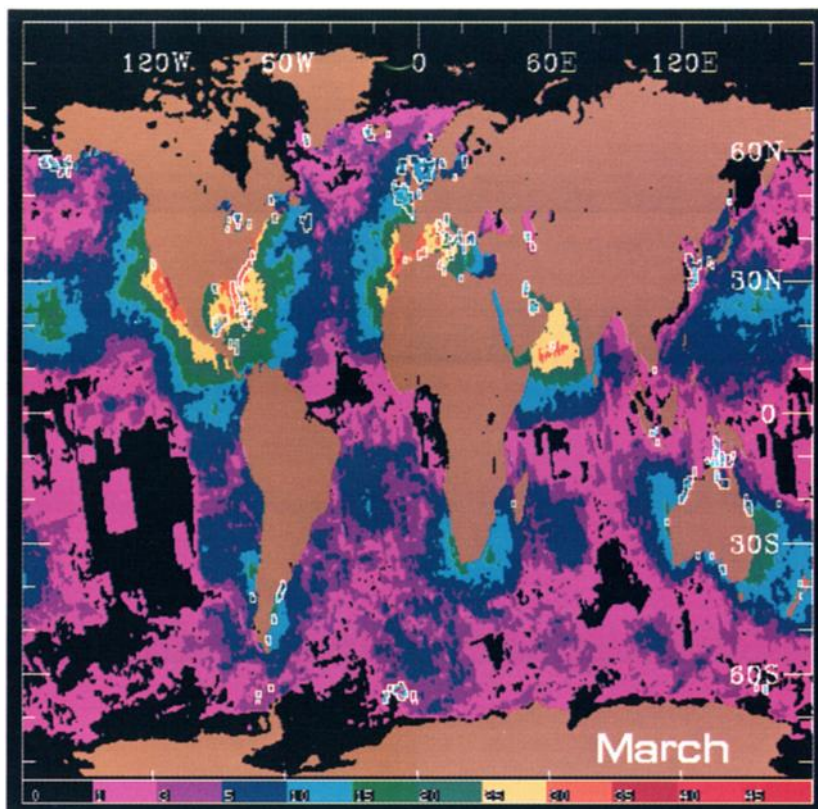

Plate 2b. Same as Plate 2a but for climatological March. March n_{max} = 48.
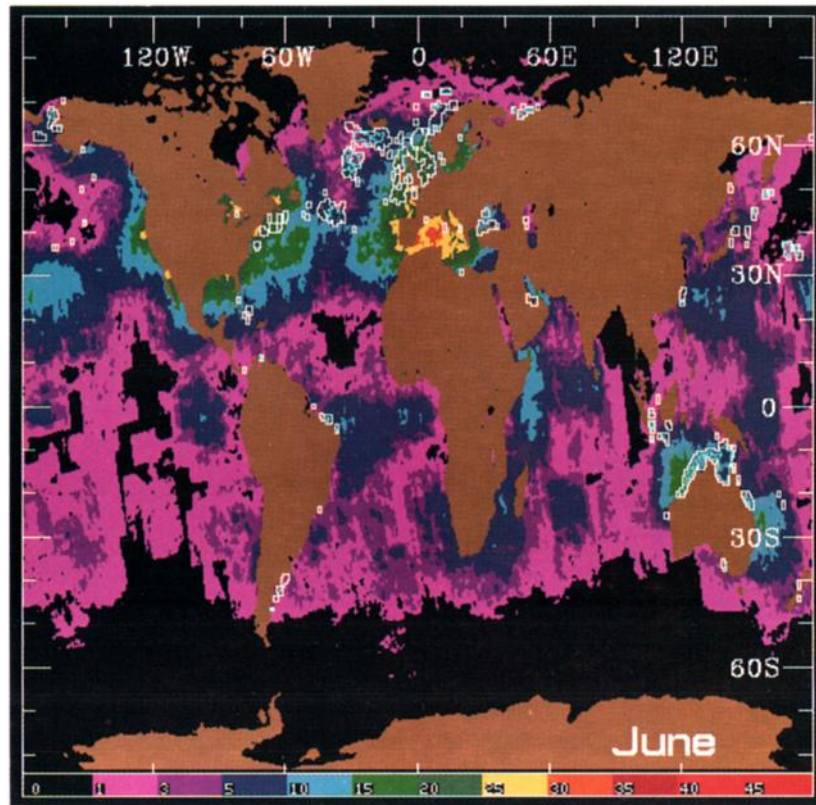
Plate 2c.   Same as Plate 2a but for climatological June. June n_{max} = 47.
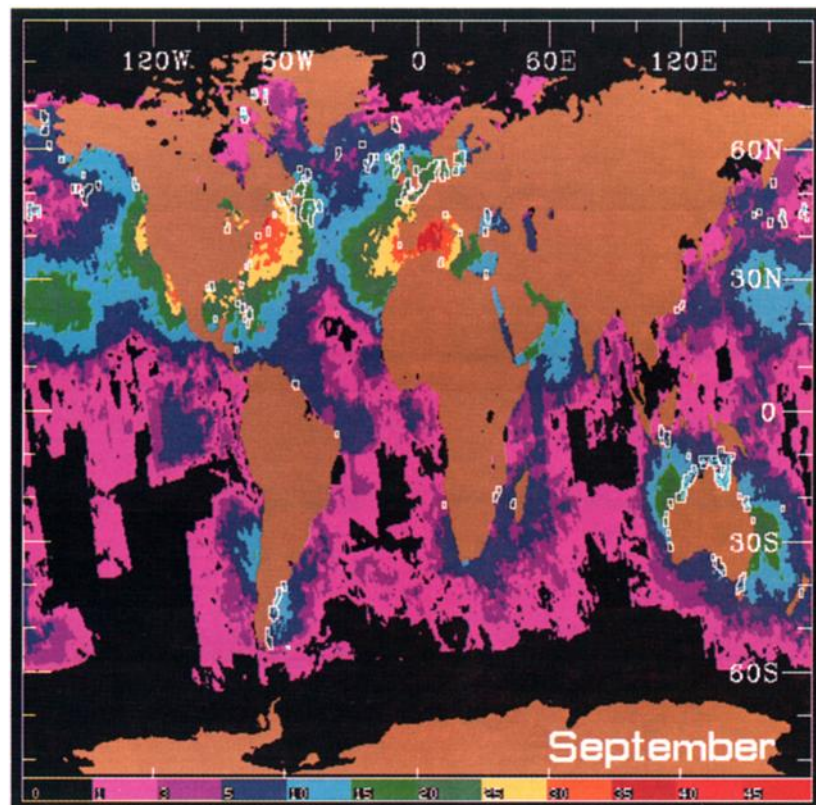
Plate 2d.   Same as Plate 2a but for climatological September. September n_{max} = 42.

tic and Gulf of Mexico. In addition to patches in the Celtic Sea, where relative frequencies attained values of 70%, patches were also apparent in the North Sea and off the western coast of Scotland and the southwest coast of Iceland. The extent of classified blooms in the Gulf of Alaska and the Bering Sea, which were only seasonally evident in imagery from 1979 to 1981 in this poorly sampled region of the North Pacific, had increased since February. During April and May, large expanses of classified blooms occurred in northern Australia, with minor activity on the Argentine shelf and along southern Australia in the Bass Strait and the eastern Great Australian Bight. By May the spatial extent of the signals in the Yellow Sea, Persian Gulf, and Gulf of Mexico was virtually nonexistent. Low activity was concentrated off the central U.S. coast, with several patches appearing in the Mid-Atlantic Bight, in the temperate-subpolar North Atlantic, and off the Norwegian coast extending north to 75°N.

During June (Plate 2c), the distribution pattern of the classified blooms in the southern hemisphere remained relatively unchanged from that observed in May. Small patches were evident on the Argentina Shelf, off the northeastern Brazilian coast, and in the vicinity of the Java and South China seas. The largest signal of the southern hemisphere was still located off northern Australia. In the northern hemisphere, classified blooms first appeared in the open ocean of the temperate-subpolar North Pacific during June. In the North Atlantic, June marked the appearance of blooms off the northeastern U.S. coast, in the Gulf of Maine and on the Nova Scotian shelf. Large expanses often remained in the open sea south of Iceland, off the coast of Norway, and surrounding the United Kingdom. The global distribution pattern during July and August remained essentially the same as in June, particularly in the southern hemisphere. The bloom signal in the polar North Pacific had decreased, with most patches now existing between 40° and 55°N. In the North Atlantic, the locations of classified bloom occurrence shifted northward, with patches in the Gulf of St. Lawrence and on the Grand Banks in the western basin, from 50° to 63°N in the central section, and in the North Sea in the eastern basin.

The size of the northern Australian and Java Sea signals had decreased by September (Plate 2d), with patches in the Bass Strait and the southeastern Great Australian Bight still evident since their initial sighting in August. The spatial extent of the signals had diminished in the North Atlantic, with the patches in the open ocean and eastern basin reduced in size more than those in the coastal waters and western basin. In the North Pacific, scattered patches between 40° and 55°N continued to be detected in September. During October and November the occurrence of classified blooms had shifted from higher latitudes in the northern hemisphere back to the Yellow Sea, Persian Gulf, and Gulf of Mexico. In the southern hemisphere, the sizes and relative probabilities of occurrence in northern Australia continued to decrease, with a concomitant increase in the number of patches off New Zealand and Argentina.

As Plates 2a to 2d indicate, the greatest areal extent of classified blooms in subpolar oceanic regions was detected during the summer to early autumn of the respective hemisphere (Figure 4b), while the maximum extent in several low-latitude marginal seas occurred during midwinter to early spring (Figure 4d). Seasons are centered on the months

of the celestial equinoxes and solstices. Percentage of exposed sea surface was provided (Figures 4a and 4c) as a proxy for the reliability of bloom areal extent. Bloom size was correlated to this measure of regional coverage in certain geographic areas, for example, the Subarctic North Atlantic (Spearman $\rho = 0.81$, $p < 0.001$), although the correlation between these two variables overall was poor but significant ($\rho = 0.28$, $p < 0.001$). Additionally, these correlations suggest that the areal extents of blooms were underestimated because the majority of visibilities were well below 100%.

A bimodal pattern in average monthly bloom extent was evident (though not significant owing to its large variability) in the subpolar northern hemisphere (Figure 4b), with a minor peak occurring in March and the major peak occurring in August, whereas the southern hemisphere region displayed a single maximum in December. In comparison, the total extent of classified blooms detected in the Gulf of Mexico and Chinese Sea appears less pronounced than that observed in the Arafura Sea and Gulf of Carpentaria, which exhibited a maximum during July (Figure 4d). The large standard deviation associated with each monthly average (Figures 4b and 4d) indicates that interannual variability of total bloom extent during a particular month was high in both the subpolar regions and the low-latitude seas.

We focused our attention on bloom signals in subpolar latitudes because the majority of these likely represent the occurrence of actual coccolithophorid blooms, whereas those detected at lower latitudes, particularly in shallow shelf environments, are likely caused by conditions that mimic the spectral signature of blooms (as will be discussed later).

Monthly totals of bloom surface area of the Subarctic North Atlantic (40°–70°N) and of the circumpolar Subantarctic and northern Antarctic (40°–60°S), representing primarily the extent of blooms on the Argentine shelf and shelf break, illustrate the interannual variability in the magnitude of the classified bloom's spatial extent within and between the subpolar regions in the northern and southern hemispheres (Figure 5). The maximum monthly (and annual) bloom surface areas of the Subarctic North Atlantic were larger during 1979–1982 than during the following years, whereas those in the Subantarctic-Antarctic were larger during 1983–1985. Additionally, extensive open ocean blooms were evident south of Iceland during June–July 1980. The variability of bloom size in the Subarctic Atlantic may be partially explained by differences in the amount of exposed sea surface because (1) the monthly bloom size was correlated to annual sea surface visibility (see above), and (2) the annual mean visibilities were statistically greatest during 1979 to 1982. Because the annual visibility in the Subantarctic followed a trend similar to that in the Subarctic North Atlantic, the interannual variability in bloom sizes in this region was not likely due to differences in the percentages of exposed sea surface in different years. In both regions, however, any correlation between sea surface visibility and total bloom extent is suspect without knowledge of the spatial distribution of exposed sea surface pixels relative to classified blooms.

Discussion

The detection of coccolithophorid blooms in this study is sensitive to light backscattered from approximately one
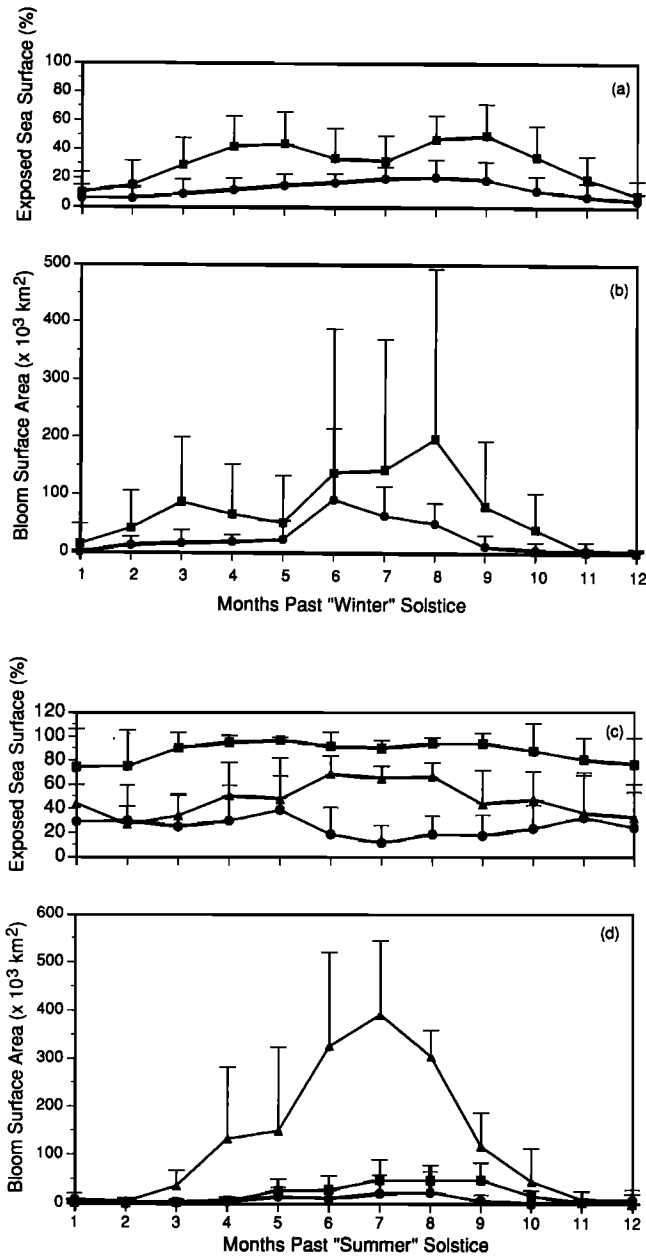
Figure 4. (a) Monthly mean percentage (+1 standard deviation) of exposed sea surface and (b) total classified coccolithophorid bloom surface area (×10³ km²) in the subpolar regions (40°–70°N, 40°–70°S) of the northern (solid boxes) and southern (solid circles) hemispheres from 1979 to 1985. Visibility is the proportion of exposed sea surface in the region. (c) Monthly mean percentage (+1 standard deviation) of exposed sea surface and (d) total classified coccolithophorid bloom surface area (×10³ km²) in the Gulf of Mexico (solid boxes), the Arafura Sea–Gulf of Carpentaria (solid triangles), and Indonesian seas (the Gulf of Thailand, South China Sea, and Java Sea) (solid circles) from 1979 to 1985. Visibility is the proportion of exposed sea surface in the region.

attenuation depth in the water column and is primarily a function of coccolith, not cell, concentrations [Balch et al., 1991]. Consequently, the results reflect the distribution pattern of coccolithophorid blooms occurring in the surface layer and are biased toward the declining stage (stationary

phase) of the bloom when the proportion of coccoliths to cells is greatest [Balch et al., 1991]. In addition, the post-classification filtering of classified blooms will bias the results to single blooms measuring greater than 4800 km². We presume that all patches recognized as blooms are composed of the coccolithophorid E. huxleyi, the only species presently documented to be visible in satellite imagery [Balch et al., 1991; Holligan and Balch, 1991].

Though blooms were efficiently separated from most non-bloom classes, classification of satellite imagery prevents unequivocal identification of the source of the detected patches. With the lack of contemporaneous sea truth to directly verify the distribution pattern of classified blooms, we evaluate the derived pattern's validity by comparing it with biogeographical information of E. huxleyi blooms and by examining the sources of error and bias in image processing, classification, and coverage.

Image Processing, Classification, and Coverage

The nonrandom distribution pattern of exposed sea surface, which is dependent on both image coverage and regional atmospheric conditions, influences the distribution pattern of blooms and the estimation of their areal extent. The low number of 5-day composites in oceanic regions and the relatively low monthly percentage of exposed sea surface, particularly at higher latitudes, where the greatest areal extent of blooms are detected, suggest that bloom occurrences may be completely missed and their areal extents may be underestimated [Brown and Yoder, 1994] and aliased with weather conditions [Abbott and Zion, 1987]. Additionally, annual differences in image coverage often account for a large proportion of the seasonal variability in estimates of total bloom size in a given region, such as the Subarctic North Atlantic.

Error may be introduced during image processing and classification. Prior to classification, incorrect water-leaving radiances will be calculated if inappropriate default parameter values and assumptions are used during atmospheric correction and may affect the outcome of classification. For example, radiances from high latitudes (>65°) may suffer from inaccurate retrieval due to high solar zenith angles and/or a combination of other reasons [Thomas and Strub, 1989]. The errors in radiance retrieval, however, are implicitly incorporated into the classification algorithm because the training, testing, and classified imagery were all processed similarly. In addition, the training pixels are biased toward conditions from the North Atlantic, suggesting that the spectral signatures of the various conditions may be inadequately characterized from a global perspective.

The classification algorithm accurately separated bloom from most nonbloom conditions at the spatial resolution of the PST imagery during testing simulations. This high degree of discrimination is presumed to apply to image classification, because the assumptions employed in the simulations are likely to be satisfied by the spatial and temporal subsampling involved in PST image generation. Still, caution is required when assigning the source of the classified bloom signal. Several nonbloom conditions, particularly whitings, can be incorrectly classified as blooms because they mimic spectral signatures. To assess this ambiguity, we compare our results with the distribution pattern of both bloom and bloom-mimicking conditions established from in situ-collected material.
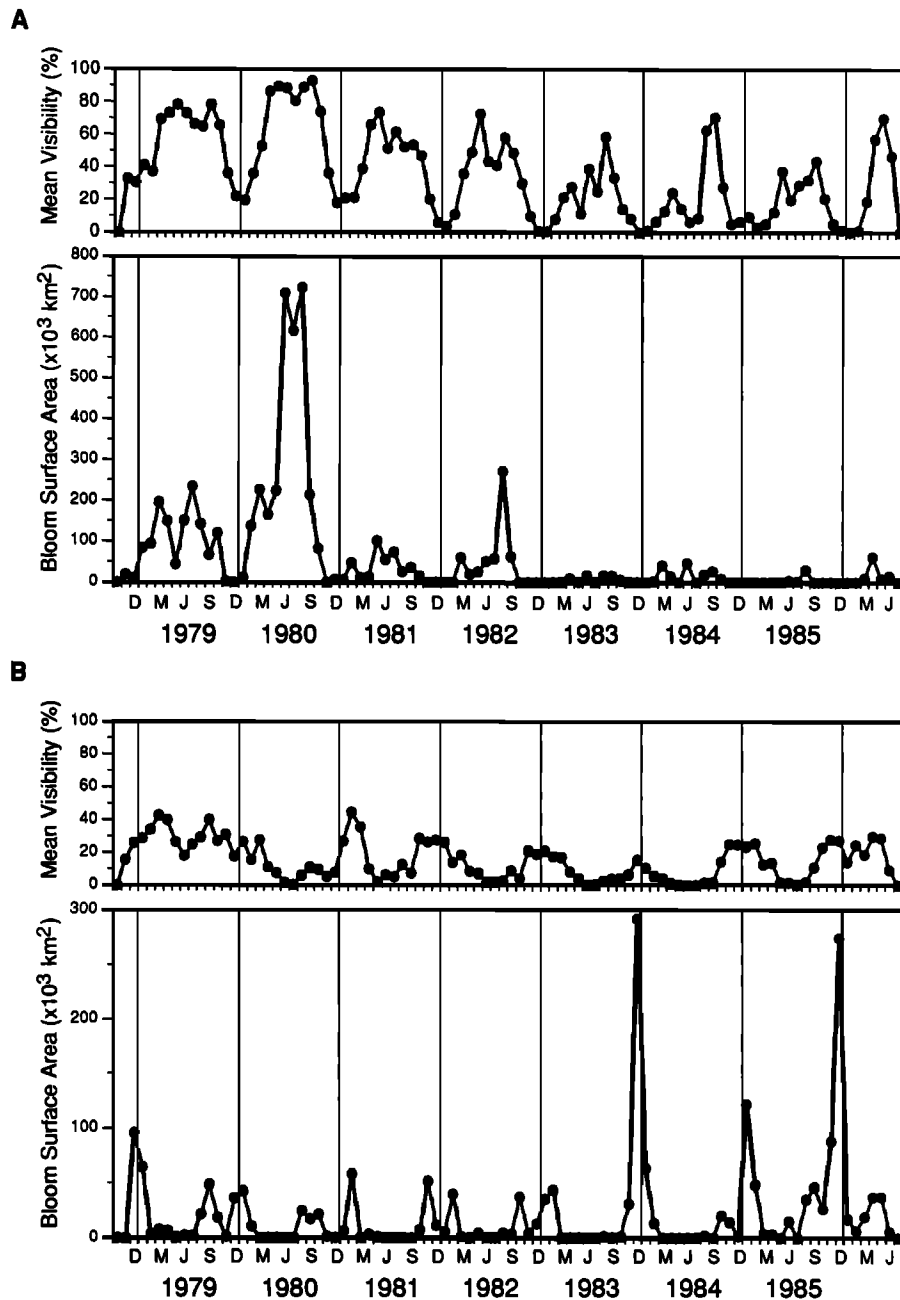
Figure 5. (top) Monthly exposed sea surface (percent) and (bottom) total surface area of classified coccolithophorid blooms ($\times 10^3$ km^2) for (A) the Subarctic North Atlantic (40°–70°N) and (B) the Subantarctic and northern Antarctic (40°–70°S) from October 1978 to June 1986. Visibility is the proportion of exposed sea surface in the region.

Biogeography of Coccolithophorid Blooms

Our distribution pattern of classified blooms at subpolar latitudes generally agrees with the occurrence of *E. huxleyi* at or near bloom concentrations ascertained in previous biogeographic investigations and leads us to conclude that the majority of bloom signals detected at these latitudes represent the presence of actual coccolithophorid blooms. As in our results for the Atlantic, high concentrations ($\geq 10^4$ L^{-1}) of *E. huxleyi* have been detected within the surface mixed layer off the coasts of eastern North America [*Ackleson and Holligan*, 1989; *Balch et al.*, 1991; *Blackwelder and*

Hooker, 1986; *Brown and Yoder*, 1993, 1994; *McIntyre and Be*, 1967; *Okada and McIntyre*, 1977, 1979], central and northern Europe to 69°N [*Berge*, 1962; *Cadée*, 1985; *Eide*, 1990; *Holligan and Groom*, 1986; *Holligan et al.*, 1983; *Milliman*, 1980; *Samtleben and Bickert*, 1990], and southern Iceland [*Geitzenauer et al.*, 1977; *Holligan et al.*, 1993] between May and October and on the Argentine Shelf in December–January [*Hentschel*, 1932, 1936]. High cell concentrations were present in surface waters of the Subarctic and Subantarctic central Pacific during August [*Okada and Honjo*, 1973] and December–January [*Hasle*, 1960], respec-

tively, and blooms were detected off Japan during May–August [*Fukushima et al.*, 1987] and off southern Tasmania (G. M. Hallegraeff, personal communication, 1992), also affirming our results. In contrast to our findings, blooms were not detected on the Celtic Shelf and in the southern Irish Sea during winter or in the southeastern Bering Sea [*Müller-Karger et al.*, 1990].

In nearshore equatorial and subtropical regions of the western Atlantic, classified blooms are also apparent in areas where *E. huxleyi* and *Gephyrocapsa oceanica* have been observed at high concentrations [*McIntyre et al.*, 1970; *Okada and McIntyre*, 1977; *Yoder*, 1983]. Off coastal South Africa and Namibia, relatively small but intense blooms (10^6 cells L^{-1}) of *E. huxleyi* or *G. oceanica*, a coccolithophore similar in size to *E. huxleyi* [*McIntyre and Be*, 1967], occur between March and August [*Mitchell-Innes and Winter*, 1987, and references therein]. In the western Pacific, *G. oceanica* dominates the monsoonally influenced regions of the equatorial and subtropical Indian Ocean and marginal seas of the Indo-Pacific with concentrations ranging from 10^3–10^5 L^{-1} [*Hallegraeff*, 1984; *Honjo*, 1977; *Houghton and Guptha*, 1991; *Okada and Honjo*, 1975]. Though not verified, *G. oceanica* blooms may account for a portion of the classified blooms detected in these regions, because they are known to discolor the water a milky white [*Grindley and Taylor*, 1970] and may be visible in satellite imagery.

The paucity of blooms in the Arabian Sea and the Indian Ocean is in agreement with findings of several older phytoplankton studies [*Subrahmanyan and Viswanatha Sarma*, 1965; *Taylor*, 1973], yet *Kleijne et al.* [1989] found up to 10^5 cells L^{-1} in the Arabian Sea during the southwestern monsoon. *Brock and McClain* [1992] also noted "obvious" coccolithophorid blooms off the north Omani coast in CZCS imagery during May–June 1982 that were not depicted in our results. This discrepancy may result from our higher threshold in the CZCS yellow band (nLw 550), though these values are not strictly comparable because different epsilon coefficients were used during atmospheric correction. These coastal regions, however, may also be more prone to harbor conditions imitating the spectral signature of blooms.

Spectrally Mimicking Conditions

Conditions which mimic the CZCS spectral signature of coccolithophorid blooms and are consequently misclassified as blooms may represent a portion of the classified blooms, particularly in shallow shelf regions at lower latitudes. We can surmise the source of this signal based on supplemental information such as regional sediment composition, but verification is tentative given the scarcity of in situ observations. Blooms of other phytoplankton species, for example, diatoms, may produce a strong reflectance at a particular wavelength (P. M. Holligan, personal communication, 1992) but are normally distinguishable from the "white" reflectance of coccolithophorid blooms because of their strong absorption in the blue spectrum. One exception to this rule includes a certain stage of cyanobacterium blooms, e.g., of *Tricodesmium*, which forms bright yellow or golden surface slicks that appear white in CZCS imagery [*Dupouy et al.*, 1988]. However, the absence of classified blooms in areas frequented by *Tricodesmium* blooms during periods of calm weather, such as the Maldive Islands in the Indian Ocean and the Coral Sea in the southwest Pacific during the austral summer [*Carpenter*, 1983a, b], suggests that the classifier

can effectively separate *Tricodesmium* from coccolithophorid blooms. In contrast, the signal in the Baltic Sea is likely due to blooms of the cyanobacterium *Nodularia* [*Ulbricht*, 1983].

As was mentioned previously, suspended sediments from rivers are often distinguishable. However, the Yellow Sea [*Wright et al.*, 1990], the coastal East China Sea, and the Louisiana-Texas shelf [*Müller-Karger et al.*, 1991] are likely exceptions.

Whitings or similar conditions are expected to be confused with blooms given the inability of the classification algorithm to resolve the two. Classified blooms in the Great Lakes likely represent the occurrence of whitings [*Strong and Eadie*, 1978], because coccolithophorids are absent from these lakes. Sedimental evidence suggests that the extensive bloom signals on or in the Yucatan and West Florida shelves, the Honduras Bank, the Bahamas, and the Arafura Sea and Gulf of Carpentaria are not due to the presence of coccolithophorid blooms. This fact and their seasonal appearance, which is coincident with stormy weather, imply that these signals are due to the (re)suspension of noncoccolith-dominated carbonate sediments [*Bhattacharyya and Friedman*, 1983; *Logan et al.*, 1970; *Milliman*, 1974; *Robbins and Blackwelder*, 1992; *Scholle et al.*, 1983; M. Furnas, personal communication, 1992; G. M. Hallegraeff, personal communication, 1992]. The paucity of sampling from these regions, however, renders the determination of the actual conditions inconclusive.

To summarize, we presume that the classified bloom detected at temperate and subpolar latitudes (35°–65°) represents the presence of actual coccolithophorid blooms. Classified blooms detected at lower latitudes, particularly in shallow coastal regions or marginal seas, are likely not to be due to the occurrence of coccolithophorids, with the possible exception of *G. oceanica* in the Indo-Pacific marginal seas. Consequently, the estimates of bloom-produced DMS and $CaCO_3$ (to be discussed later) are conservatively based only on blooms detected in the Subarctic latitudes.

Whatever the source of the classified bloom signal, the large areas affected by these signals emphasize the need to identify and spectrally characterize the conditions responsible for them. These high-reflectance conditions profoundly affect the optical properties of the surface layer [*Aiken et al.*, 1992; *Holligan and Balch*, 1991]. For example, satellite-derived pigment concentrations from these regions are likely to be biased using the current CZCS pigment and atmospheric correction algorithms [*Balch et al.*, 1989; *Gordon et al.*, 1988b; *Holligan et al.*, 1983]. Future ocean color sensors, such as the sea-viewing wide-field-of-view sensor (SeaWiFS) and moderate-resolution imaging spectrometer (MODIS-N), with their capability for improved atmospheric correction and spectral characterization [*Hooker et al.*, 1992], will alleviate many of the current problems associated with CZCS imagery and may allow blooms to be spectrally resolved from these mimicking signals.

Bloom Temporal and Spatial Variability

The observed distribution pattern of blooms (Plate 1) is dependent upon circumstances favorable to their formation and detection. The absence of blooms in the open oceans at lower latitudes may be explained by the shift of the coccolithophorid's population to greater depths [*McIntyre and Be*, 1967; *Okada and Honjo*, 1973] than that sensed by the

CZCS. More likely, their absence is caused by the lack of environmental conditions necessary for their formation. The predominance of coccolithophorid blooms in the Subarctic North Atlantic may arise in part from the region's relatively low concentration of dissolved silicate compared to that found at similar latitudes in other ocean basins [Armstrong, 1965; Broecker and Peng, 1982], thus favoring a flagellate (coccolithophorid)-dominated phytoplankton community over a silicate-based diatom one. This reasoning is corroborated on both a local and a global scale. Locally, the highest coccolithophorid concentrations of a region have generally occurred in "aged" upwelling waters likely depleted in silicate [Betzer et al., 1977; Kleijne et al., 1989; Mitchell-Innes and Winter, 1987]. Globally, the paucity of opal sediments in the North Atlantic suggests lower diatom productivity in these surface waters than in other ocean basins [Leinen et al., 1986]. Yet the differences in the factors affecting burial of both $CaCO_3$ and silicate between oceans [Broecker and Peng, 1982], the presence of a coastal and oceanic E. huxleyi ecophenotype with potentially different nutrient requirements [van Bleijswijk et al., 1991], and the uncertainty of bloom size estimates in different regions because of variable image coverage permit only conjecture about the source of the differences in geographical occurrence of coccolithophorid blooms.

Documenting any long-term trend in the bloom's occurrence and areal extent is limited by the relatively recent advent of satellite imagery and, as previously noted, is often unreliable because these two variables are biased by image and cloud coverage. Over the past 15 or so years that visible satellite imagery has been available, extensive open ocean blooms in the Subarctic North Atlantic have appeared only twice, once in 1980 (this study) and again in 1991 [Holligan et al., 1993]. During the summer months this region is beset by clouds, which hinder the accurate assessment of the bloom's occurrence and size. In regions where the annual variability of bloom surface area is not attributable to differences in image coverage, the variation could be used to identify the environment conditions favorable for bloom occurrence. In the Subantarctic–northern Antarctic (Figure 5), for example, preliminary analysis indicated that blooms were not correlated to anomalies in average global and hemispheric temperatures of the lower atmosphere [Spencer and Christy, 1990] or the presence of El Niño in the Pacific and Atlantic oceans [Horel et al., 1986; Philander, 1990].

Biogeochemical Influence

Though the biological response of regions affected by coccolithophorid blooms is beyond the scope of this paper, the large area covered by blooms undoubtedly affects the ecology of the region by decreasing the depth of its photic zone [Ackleson and Holligan, 1989; Holligan and Balch, 1991] and modifying the chemistry of its surface water through coccolith and DMS formation.

The presumed E. huxleyi blooms detected at subpolar latitudes, as defined in Table 3, are estimated to produce an average of 0.4–1.3×10^6 t calcite carbon ($CaCO_3$-C) and 10,000 t DMS sulfur (DMS-S) annually. These estimates are based on standing stock calculations using the mean annual areal extent of the blooms (1.0×10^6 km^2) and assuming a mixed layer 20 m deep with 0.02–0.065 g $CaCO_3$-C m^{-3} [Balch et al., 1992; Brown and Yoder, 1994], 2000 E. huxleyi cells mL^{-1} [Balch et al., 1991], and 1.10 pg DMSP cell^{-1}

[Keller, 1989]. These estimates do not include the contribution of $CaCO_3$ and DMS from coccolithophorid populations not detected by our classification algorithm. They also represent minimum yields owing to the conservative assumptions employed in the standing stock calculations. Estimates of both DMS-S and $CaCO_3$-C production would increase approximately 1 order of magnitude if we included the turnover and loss of cells and coccoliths from the mixed layer in our calculations.

Nevertheless, the flux of $CaCO_3$ to the sediments and of DMS to the atmosphere is likely to be large in regions occupied by blooms. The subpolar regions, constituting approximately 25% of the global ocean, supply almost three quarters of these bloom-produced compounds. In addition, the calcite carbon production estimates translate into relatively large fluxes (13–33 mg $CaCO_3$-C m^{-2} d^{-1} [Brown and Yoder, 1994] that would be most extensive during or immediately following the period of the blooms greatest areal extent, for example, summer and early autumn in the subpolar region. The estimated DMS concentration in bloom waters (i.e., 16.4 nmol DMS-S L^{-1}) is approximately 5 times higher than the global mean concentration of 3.1 nmol DMS-S L^{-1} [Andreae, 1986], implying a sea-to-air flux of similar magnitude. The satellite-derived pattern of blooms does not accurately predict the magnitude or timing of this atmospheric flux because it is not based on variables relevant to these variables, such as cell biomass or physiological state. However, since coccolithophorids are one of the principal producers of DMS among the phytoplankton, our results provide a map of presumed "hot spots" of DMSP/DMS production on a monthly to seasonal scale which can be used to supplement methods attempting to estimate the magnitude of DMS sea-to-air flux based on phytoplankton biomass [Thompson et al., 1990].

On a global scale, however, the satellite-detected coccolithophorid blooms play only a minor role in the annual flux of $CaCO_3$ and DMS from the mixed layer to depth or the atmosphere, respectively. The estimated DMS-S produced by blooms located in the subpolar regions represents only a small fraction (0.03–0.07%) of the estimated 0.5 to 1.1 Tmol DMS-S yr^{-1} (Tmol = 32×10^{12} g) [Andreae, 1986; Bates et al., 1987b] emitted to the atmosphere (making the unrealistic assumption that all of the estimated DMS produced is ventilated). Similarly, calcite-carbon production at these latitudes, assuming no coccolith dissolution in the water column, accounts for at most 0.3% of the 0.4–1.4×10^9 t $CaCO_3$-C annual global sediment flux from the mixed layer [Sundquist, 1985]. This conclusion suggests that the majority of coccoliths making up the pelagic carbonate sediments are derived from populations not detected in the CZCS imagery.

The formation of coccoliths by blooms at high latitudes in the North Atlantic, a region of the global ocean known to be important to atmospheric CO_2 drawdown [Sarmiento and Toggweiler, 1984; Siegenthaler and Wenk, 1984], decreases the relative air-to-sea CO_2 flux by increasing surface layer pCO_2 [Taylor et al., 1991]. The bloom's influence on this flux hinges upon the timing, extent, and density of coccolith production and its relation to periods of maximum atmospheric CO_2 exchange. With the potential of being able to estimate coccolith concentration, and subsequently surface layer pCO_2, from satellite imagery [Aiken et al., 1992; Gordon et al., 1988b; Holligan et al., 1993], the magnitude and pattern of this mediating effect on the air-to-sea CO_2 flux

caused by coccolithophorid blooms may be measured directly from space in the near future.

Conclusion

Surface waters with the relatively unique spectral signature of coccolithophorid blooms annually covered an average of 1.4×10^6 km^2 in the global ocean, with those in subpolar latitudes, particularly in the North Atlantic, accounting for 71% of this surface area. Findings about blooms detected at these higher latitudes are relatively well supported by previous biogeographic investigations. On the other hand, large expanses of the bloom signal observed in numerous lower latitude marginal seas, particularly the Arafura Sea, Gulf of Carpentaria, and shelf regions in the Gulf of Mexico, may be due to the presence of coccolithophorid blooms or conditions which spectrally mimic them.

Classified blooms at subpolar latitudes achieved their largest areal extent during the months that corresponded to summer and early autumn in the respective hemispheres, while blooms at equatorial and subtropical latitudes were largest from midwinter to spring.

Standing stock estimates suggest that presumed E. huxleyi blooms act as a significant source of calcite carbon and DMS sulfur on a regional scale. On a global scale, however, the coccolithophorid blooms detected in CZCS imagery are estimated to play only a minor role in the annual production of calcite and DMS and their flux from the surface mixed layer to depth and the atmosphere, respectively.

References

Abbott, M. R., and P. M. Zion, Spatial and temporal variability of phytoplankton pigment off northern California during Coastal Ocean Dynamics Experiment 1, *J. Geophys. Res.*, *92*(C2), 1745–1755, 1987.

Ackleson, S. G., and P. M. Holligan, AVHRR observations of a Gulf of Maine coccolithophorid bloom, *Photogramm. Eng. Remote Sens.*, *55*(4), 473–474, 1989.

Aiken, J., G. F. Moore, and P. M. Holligan, Remote sensing of oceanic biology in relation to global climate change, *J. Phycol.*, *28*, 579–590, 1992.

Andreae, M. O., The ocean as a source of atmospheric sulfur compounds, in *The Role of Air-Sea Exchange in Geochemical Cycling*, edited by P. Buat-Menard, pp. 331–362, D. Reidel, Norwell, Mass., 1986.

Armstrong, F. A. J., Silicon, in *Chemical Oceanography*, edited by J. P. Riley and G. Skirrow, pp. 409–432, Academic, San Diego, Calif., 1965.

Balch, W. M., R. W. Eppley, M. R. Abbott, and F. M. H. Reid, Bias in satellite-derived pigment measurements due to coccolithophores and dinoflagellates, *J. Plankton Res.*, *11*(3), 575–581, 1989.

Balch, W. M., P. M. Holligan, S. G. Ackleson, and K. J. Voss,

Biological and optical properties of mesoscale coccolithophore blooms in the Gulf of Maine, *Limnol. Oceanogr.*, *36*(4), 629–643, 1991.

Balch, W. M., P. M. Holligan, and K. A. Kilpatrick, Calcification, photosynthesis and growth of the bloom-forming coccolithophore, *Emiliania huxleyi*, *Cont. Shelf Res.*, *12*(12), 1353–1374, 1992.

Bates, T. S., R. J. Charlson, and R. H. Gammon, Evidence for the climatic role of marine biogenic sulphur, *Nature*, *329*, 319–321, 1987a.

Bates, T. S., J. D. Cline, R. H. Gammon, and S. R. Kelly-Hansen, Regional and seasonal variations in the flux of oceanic dimethylsulfide to the atmosphere, *J. Geophys. Res.*, *92*(C3), 2930–2938, 1987b.

Berge, G., Discoloration of the sea due to *Coccolithus huxleyi* "bloom," *Sarsia*, *6*, 27–40, 1962.

Betzer, P. R., D. W. Eggimann, K. L. Carder, D. R. Kester, and S. B. Betzer, Seasonal patterns in suspended calcium carbonate concentrations during the dry and wet seasons in the eastern Caribbean, in *The Fate of Fossil Fuel CO_2 in the Oceans*, edited by N. R. Andersen and A. Malahoff, pp. 63–79, Plenum, New York, 1977.

Bhattacharyya, J., and G. M. Friedman (Eds.), *Modern Carbonate Environments*, p. 376, Hutchinson Ross, Stroudsburg, Pa., 1983.

Blackwelder, P. L., and S. Hooker, Summaries of data of a geologically significant phytoplankton subset from three warm core rings and the western North Atlantic (September 1981–October 1982), *NOVA-86-1*, 109 pp., Nova University, Ft. Lauderdale, Fla., 1986.

Bramlette, M. N., Significance of coccolithophorids in calcium carbonate deposition, *Bull. Geol. Soc. Am.*, *69*(1), 121–126, 1958.

Brock, J. C., and C. R. McClain, Interannual variability in phytoplankton blooms observed in the northwestern Arabian Sea during the southwest monsoon, *J. Geophys. Res.*, *97*(C1), 733–750, 1992.

Broecker, W. S., and T.-H. Peng, *Tracers in the Sea*, 690 pp., Lamont-Doherty Earth Observatory, Palisades, N. Y., 1982.

Brown, C. W., Distribution patterns of coccolithophorid blooms and their biogeochemical significance, Ph.D. dissertation, Univ. of R. I., Kingston, 1993.

Brown, C. W., and J. A. Yoder, Blooms of *Emiliania huxleyi* (Prymnesiophyceae) in surface waters of the Nova Scotian shelf and the Grand Bank, *J. Plankton Res.*, *18*(12), 1429–1438, 1983.

Brown, C. W., and J. A. Yoder, The distribution pattern of coccolithophorid blooms in the western North Atlantic, *Cont. Shelf Res.*, *14*(213), 175–198, 1994.

Cadée, G. C., Macroaggregates of *Emiliania huxleyi* in sediment traps, *Mar. Ecol. Prog. Ser.*, *24*, 193–196, 1985.

Carpenter, E. J., Nitrogen fixation by marine *Oscillatoria* (*Trichodesmium*) in the world's oceans, in *Nitrogen in the Marine Environment*, edited by E. J. Carpenter and D. G. Capone, pp. 65–104, Academic, San Diego, Calif., 1983a.

Carpenter, E. J., Physiology and ecology of marine planktonic *Oscillatoria* (*Trichodesmium*), *Mar. Biol. Lett.*, *4*, 69–85, 1983b.

Charlson, R. J., J. E. Lovelock, M. O. Andreae, and S. G. Warren, Oceanic phytoplankton, atmospheric sulphur, cloud albedo and climate, *Nature*, *326*, 655–661, 1987.

Dupouy, C., M. Petit, and Y. Dandonneau, Satellite detected cyanobacteria bloom in the southwestern tropical Pacific, *Int. J. Remote Sens.*, *9*(3), 389–396, 1988.

Durkee, P. A., F. Pfeil, E. Frost, and R. Shema, Global analysis of aerosol-particle characteristics, *Atmos. Environ., Part A*, *25*(11), 2457–2471, 1991.

Eide, L. K., Distribution of coccoliths in surface sediments in the Norwegian-Greenland Sea, *Mar. Micropaleontol.*, *16*, 65–75, 1990.

Feldman, G., et al., Ocean color: Availability of the Global Data Set, *Eos Trans. AGU*, *70*(23), 634–635, 640–641, 1989.

Fukushima, H., K. Hiramatsu, and Y. Sugimori, CZCS-derived pigment concentration fields in Japanese coastal area, *Adv. Space Res.*, *7*(2), 79–82, 1987.

Gaarder, K. R., Comments on the distribution of coccolithophorids in the oceans, in *The Micropalaeontology of Oceans*, edited by B. M. Funnel and W. R. Riedel, pp. 97–103, Cambridge University Press, New York, 1971.

Geitzenauer, K. R., M. B. Roche, and A. McIntyre, Coccolith

biogeography from North Atlantic and Pacific surface sediments, in *Oceanic Micropalaeontology*, edited by A. T. S. Ramsay, pp. 973–1008, Academic, San Diego, Calif., 1977.

Gordon, H. R., J. W. Brown, and R. H. Evans, Exact Rayleigh scattering calculations for use with the Nimbus-7 coastal zone color scanner, *Appl. Op.*, *27*(5), 862–871, 1988a.

Gordon, H. R., O. B. Brown, R. H. Evans, J. W. Brown, R. C. Smith, K. S. Baker, and D. K. Clark, A semianalytic radiance model of ocean color, *J. Geophys. Res.*, *93*(D9), 10,909–10,924, 1988b.

Grindley, J. R., and F. J. R. Taylor, Factors affecting plankton blooms in False Bay, *Trans. R. Soc. S. Afr.*, *39*, 201–210, 1970.

Hallegraeff, G. M., Coccolithophorids (calcareous nanoplankton) from Australia waters, *Bot. Mar.*, *27*, 229–247, 1984.

Hasle, G. R., Plankton coccolithophorids from the subantarctic and equatorial Pacific, *Nytt Mag. Bot.*, *8*, 77–88, 1960.

Hentschel, E., Die biologischen Methoden und das biologische Beobachtungsmaterial, *Wiss. Ergeb. Dtsch. Atl. Exped. Meteor*, *10*, 274, 1932.

Hentschel, E., Allgemeine Biologie des sudatlantischen Ozeans, *Wiss. Ergeb. Dtsch. Atl. Exped. Meteor*, *11*, 344, 1936.

Holligan, P. M., and W. M. Balch, From the ocean to cells: Coccolithophore optics and biogeochemistry, in *Particle Analysis in Oceanography*, edited by S. Demers, pp. 301–324, Springer-Verlag, New York, 1991.

Holligan, P. M., and S. B. Groom, Phytoplankton distributions along the shelf break, *Proc. R. Soc. Edinburgh, Sect. B, Biol. Sci.*, *88*, 239–263, 1986.

Holligan, P. M., M. Viollier, D. S. Harbour, P. Camus, and M. Champagne-Philippe, Satellite and ship studies of coccolithophore production along a continental shelf edge, *Nature*, *304*, 339–342, 1983.

Holligan, P. M., et al., A biogeochemical study of the coccolithophore *Emiliania huxleyi* in the North Atlantic, *Global Biogeochem. Cycles*, *7*(4), 879–900, 1993.

Honjo, S., Biogeography and provincialism of living coccolithophorids in the Pacific Ocean, in *Oceanic Micropalaeontology*, edited by A. T. S. Ramsay, pp. 951–972, Academic, San Diego, Calif., 1977.

Hooker, S. B., W. E. Esaias, G. C. Feldman, W. W. Gregg, and C. R. McClain, An Overview of SeaWiFS and Ocean Color, SeaWiFS Tech. Rep. 1, 24 pp., Goddard Space Flight Center, Greenbelt, Md., 1992.

Horel, J. D., V. E. Kousky, and M. T. Kagano, Atmospheric conditions in the Atlantic sector during 1983 and 1984, *Nature*, *322*, 248–251, 1986.

Houghton, S. D., and M. V. S. Guptha, Monsoonal and fertility controls on recent marginal sea and continental shelf coccolith assemblages from the western Pacific and northern Indian oceans, *Mar. Geol.*, *97*, 251–259, 1991.

Jain, A. K., *Fundamentals of Digital Image Processing*, 569 pp., Prentice-Hall, Englewood Cliffs, N. J., 1989.

Keller, M. D., Dimethyl sulfide production and marine phytoplankton: The importance of species composition and cell size, *Biol. Oceanogr.*, *6*, 375–382, 1989.

Kleijne, A., D. Kroon, and W. Zevenboom, Phytoplankton and foraminiferal frequencies in northern Indian Ocean and Red Sea surface waters, *Neth. J. Sea Res.*, *24*(4), 531–539, 1989.

Leinen, M., D. Cwienk, G. R. Heath, P. E. Biscaye, V. Kolla, and J. Thiede, Distribution of biogenic silica and quartz in recent deep-sea sediments, *Geology*, *14*, 199–203, 1986.

Logan, B. W., G. R. Davies, J. F. Read, and D. E. Cebulski, *Carbonate Sedimentation and Environments, Shark Bay, Western Australia*, 223 pp., Collegiate Press, Menasha, Wis., 1970.

McClain, C. R., W. E. Esaias, G. C. Feldman, J. Elrod, D. Endres, J. Firestone, M. Darzi, R. Evans, and J. Brown, Physical and biological processes in the North Atlantic during the First GARP Global Experiment, *J. Geophys. Res.*, *95*(C10), 18,027–18,048, 1990.

McIntyre, A., and A. Be, Modern Coccolithophoridae of the Atlantic Ocean, I, Placoliths and crytoliths, *Deep Sea Res.*, *14*, 561–597, 1967.

McIntyre, A., A. Be, and M. B. Roche, Modern Pacific coccolithophorids: A paleontological thermometer, *Trans. N. Y. Acad. Sci. Ser. 2*, *32*(6), 720–731, 1970.

Milliman, J. D., *Marine Carbonates*, 375 pp., Springer-Verlag, New York, 1974.

Milliman, J. D., Coccolithophorid production and sedimentation, Rockall Bank, *Deep Sea Res., Part A*, *27*, 959–963, 1980.

Mitchell-Innes, B. A., and A. Winter, Coccolithophores: A major phytoplankton component in mature upwelled waters off the Cape Peninsula, South Africa in March, 1983, *Mar. Biol.*, *95*, 25–30, 1987.

Mueller, J. L., Nimbus-7 CZCS: Electronic overshoot due to cloud reflectance, *Appl. Opt.*, *27*, 438–440, 1988.

Müller-Karger, F. E., C. R. McClain, R. N. Sambrotto, and G. C. Ray, A comparison of ship and coastal zone color scanner mapped distribution of phytoplankton in the southeastern Bering Sea, *J. Geophys. Res.*, *95*(C7), 11,483–11,499, 1990.

Müller-Karger, F. E., J. J. Walsh, R. H. Evans, and M. B. Meyers, On the seasonal phytoplankton concentration and sea surface temperature cycles of the Gulf of Mexico as determined by satellites, *J. Geophys. Res.*, *96*(C7), 12,645–12,665, 1991.

Okada, H., and S. Honjo, The distribution of oceanic coccolithophorids in the Pacific, *Deep Sea Res.*, *20*, 355–374, 1973.

Okada, H., and S. Honjo, Distribution of coccolithophores in marginal seas along the western Pacific Ocean and Red Sea, *Mar. Biol.*, *31*, 271–285, 1975.

Okada, H., and A. McIntyre, Modern coccolithophores of the Pacific and North Atlantic oceans, *Micropaleontology*, *23*, 1–55, 1977.

Okada, H., and A. McIntyre, Seasonal distribution of modern coccolithophores in the western North Atlantic Ocean, *Mar. Biol.*, *54*, 319–328, 1979.

Philander, S. G., *El Niño, La Niña, and the Southern Oscillation, Int. Geophys. Ser.*, vol. 46, 293 pp., Academic, San Diego, Calif., 1990.

Robbins, L. L., and P. L. Blackwelder, Biochemical and ultrastructural evidence for the origin of whitings: A biologically induced calcium carbonate precipitation mechanism, *Geology*, *20*, 464–468, 1992.

Samtleben, C., and T. Bickert, Coccoliths in sediment traps from the Norwegian Sea, *Mar. Micropaleontol.*, *16*, 39–64, 1990.

Sarmiento, J. L., and J. R. Toggweiler, A new model for the role of the oceans in determining atmospheric p_{CO_2}, *Nature*, *308*, 621–624, 1984.

Sarmiento, J. L., J. R. Toggweiler, and R. Najjar, Ocean carbon-cycle dynamics and atmospheric pCO_2, *Philos. Trans. R. Soc. Lond., Ser. A*, *325*, 3–21, 1988.

SAS Institute, *SAS User's Guide: Statistics*, 5th ed., 956 pp., Cary, N. C., 1985.

Scholle, P. A., D. G. Bebout, and C. H. Moore (Eds.), *Carbonate Depositional Environments*, 704 pp., American Association of Petroleum Geologists, Tulsa, Okla., 1983.

Schowengerdt, R. A., *Techniques for Image Processing and Classification in Remote Sensing*, 249 pp., Academic, San Diego, Calif., 1983.

Shinn, J. A., R. P. Steinen, B. H. Lidz, and P. K. Swart, Whitings, a sedimentologic dilemma, *J. Sediment. Petrol.*, *59*(1), 147–161, 1989.

Siegenthaler, U., and T. Wenk, Rapid atmospheric CO_2 variations and ocean circulation, *Nature*, *308*, 624–626, 1984.

Simpson, J. J., Image masking using polygon fills and morphological transformations, *Remote Sens. Environ.*, *40*, 161–183, 1992.

Spencer, R. W., and J. R. Christy, Precise monitoring of global temperature trends from satellites, *Science*, *247*, 1558–1562, 1990.

Strong, A. E., and B. J. Eadie, Satellite observations of calcium carbonate precipitations in the Great Lakes, *Limnol. Oceanogr.*, *23*(5), 877–887, 1978.

Subrahmanyan, R., and A. H. Viswanatha Sarma, Studies on the phytoplankton of the west coast of India, IV, Magnitude of the standing crop for 1955–1962, with observations on nanoplankton and its significance to fisheries, *J. Mar. Biol. Assoc. India*, *7*(2), 406–419, 1965.

Sundquist, E. T., Geological perspective on carbon dioxide and the carbon cycle, in *The Carbon Cycle and Atmospheric CO_2: Natural Variations Archean to Present, Geophys. Monogr. Ser.*, vol. 32, edited by E. T. Sundquist and W. S. Broecker, pp. 5–60, AGU, Washington, D. C., 1985.

Taylor, A. H., A. J. Watson, M. Ainsworth, J. E. Robertson, and D. R. Turner, A modelling investigation of the role of phytoplank-

ton in the balance of carbon at the surface of the North Atlantic, *Global Biogeochem. Cycles, 5*(2), 151–171, 1991.

Taylor, F. J. R., General features of dinoflagellate material collected by the "Anton Bruun" during the International Indian Ocean Expedition, in *The Biology of the Indian Ocean*, edited by B. Zeitzschel, pp. 155–169, Springer-Verlag, New York, 1973.

Thomas, A. C., and P. T. Strub, Interannual variability in phytoplankton pigment distribution during the spring transition along the West Coast of North America, *J. Geophys. Res., 94*(C12), 18,095–18,117, 1989.

Thompson, A. M., W. E. Esaias, and R. L. Iverson, Two approaches to determining the sea-to-air flux of dimethyl sulfide: Satellite ocean color and a photochemical model with atmospheric measurements, *J. Geophys. Res., 95*(D12), 20,551–20,558, 1990.

Ulbricht, K. A., Comparative experimental study on the use of original and compressed multispectral Landsat data for applied research, *Int. J. Remote Sens., 4*(3), 571–582, 1983.

van Bleijswijk, J., P. van der Wal, R. Kempers, M. Veldhuis, J. R. Young, G. Muyzer, E. de Vrind-de Jong, and P. Westbroek, Distribution of two types of *Emiliania huxleyi* (Prymnesiophyceae) in the Northeast Atlantic region as determined by immunofluorescence and coccolith morphology, *J. Phycol., 27*, 566–570, 1991.

Wallace, J. M., and P. V. Hobbs, *Atmospheric Science*, 467 pp., Academic, San Diego, Calif., 1977.

Wright, L. D., W. J. J. Wiseman, Z.-S. Yang, B. D. Bornhold, G. H. Keller, D. B. Prior, and J. N. Suhayda, Processes of marine dispersal and deposition of suspended silts off the modern mouth of the Huanghe (Yellow River), *Cont. Shelf Res., 10*(1), 1–40, 1990.

Yoder, J. A., Primary production in Loop Current upwelling, in Southwest Florida Shelf Ecosystem Study, Year 2, Final Report, Hydrography and Primary Productivity, contract 14-12-0001-29144, pp. 227–283, Miner. Manage. Serv., U.S. Dep. of the Inter., Washington, D. C., 1983.

C. W. Brown, NASA Goddard Space Flight Center, Code 971, Greenbelt, MD 20771.

J. A. Yoder, Graduate School of Oceanography, University of Rhode Island, Narragansett, RI 02882.